A Novel Frequency Selective Surface Loaded MIMO Antenna with Low Mutual Coupling and Enhanced Gain

Habib Ullah, Qunsheng Cao*, Ijaz Khan, Saeed U. Rahman, and Adamu H. Jabire

Abstract—This study focuses on the utilization of a slotted patch MIMO antenna to enhance isolation and gain. The MIMO antenna configuration includes two radiators integrated with an array of Frequency Selective Surfaces (FSSs). These antenna components are implemented on an FR-4 substrate and encompassed by FSS units that are optimized for X-band frequencies. The proposed MIMO antenna possesses dimensions of 65 mm (width) × 45 mm (length) × 1.6 mm (height). The primary objective of incorporating FSSs is to not only enhance isolation but also achieve high gain. The proposed FSS design features a circular ring structure with a rectangular loop at its center. The FSS unit cells exhibit excellent stability across various polarization incidence angles and operate within the frequency range of 7 to 9 GHz. The FSS loaded antenna offers a bandwidth ranging from 8.0 to 8.55 GHz, with a peak gain of 6.5 dB and isolation exceeding −20 dB among the MIMO elements. Furthermore, the study explores the MIMO antenna's performance in terms of diversity gain (DG), efficiency, and Envelope Correlation Coefficient (ECC), demonstrating superior results compared to existing state-of-the-art approaches. The proposed findings are validated by fabricating a sample prototype and conducting a comprehensive comparison between simulated and measured results.

1. INTRODUCTION

Microstrip patch antennas (MPAs) have gained significant attention for high-frequency data communication in various applications. They are favored for their lightweight design, cost-effectiveness, and ease of fabrication. However, their large size limits their utilization in multiple-input multiple-output (MIMO) antenna systems. Although traditional MPAs can be employed for 5G networks, their compact size often leads to a narrow bandwidth [1]. The emergence of 5G systems promises seamless connectivity for cutting-edge technologies such as virtual reality, smart homes, telehealth, and the Internet of Vehicles (IoV). In the current communication landscape, MIMO antennas play a crucial role in transmitting and receiving multiple data streams within the same radio network [2]. Because they reduce interference, MIMO antennas are a critical element in modern wireless communication networks because they increase connection quality and channel capacity without needing additional bandwidth. Designing MIMO antennas is a substantial challenge since electromagnetic wave interactions among close components can affect antenna properties, including bandwidth, gain enhancement, and radiation pattern [3]. MIMO antenna system is an exciting research area that may be utilized to increase the range and dependability of Wi-Fi LAN, Bluetooth, PDAs, DCS, WLAN, and UMTs. It is also important for the deployment of next-generation wireless equipment. Surface wave and near-field effects cause coupling between antenna components, which has a direct impact on the presentation of the array. So, in many MIMO antenna applications, mutual coupling cannot be neglected [4, 5]. The mutual coupling problem between antenna components is difficult to resolve using baseband algorithms and signal processing.

To minimize mutual coupling, a minimum distance between adjacent patches is required [6]. Several techniques for lowering mutual coupling have been studied to solve this problem, including stub loading technique [7], defected ground structure (DGS) [8], electromagnetic band gap (EBG) structure [9, 10], neutralization lines [11], resonator structures [12], slots [13], and metamaterial [14]. Several other techniques for enhancing the gain of microstrip antennas have also been reported, including antennas with substrates [15], superstrates [16, 17], reflective surfaces [16–20], and metamaterials [21]. In recent times, FSSs are mainly two-dimensional arrays of dielectric patches or aperture arrays within a metallic screen that perform the appropriate filtering action [22]. Another FSS composed only of dielectrics is acceptable for wideband near-field correction, beam scanning, and other applications requiring a lot of bandwidth [23, 24]. For about 50 years, FSS has been analyzed. The FSS may be used to improve the gain and directivity of patch antennas. FSSs are periodic arrays made up of conductive patches or aperture components that, depending on their frequency, reflect or transmit electromagnetic waves. They operate as spatial filters, allowing electromagnetic waves to pass through or bounce back. They are often used as antenna reflectors due to their band-stop or band-pass characteristics [25], Radom [26], electromagnetic absorbers [27], radar cross-section reduction elements [28], and artificial magnetic conductors [29]. One current challenge is suppressing spurious bands while improving antenna gain. Several approaches for increasing gain in MIMO antennas have been studied. In [30], for MIMO system gain and isolation advancements, a current metamaterial (MTM)-based superstructure is studied. In [31], a dual-band rectangular microstrip antenna with decoupling structures is proposed; the decoupling structure consists of modified array antenna decoupling surface (MADS) and H-shaped defect ground structures (HDGS). Under the impact of the MADS, the gain is increased in the work bands. In [32], a symmetrical dual-beam end-fire bow-tie antenna with gain improvement for 5G MIMO applications is designed by merging three pairs of MTM arrays. In [33], a single-layer substrate integrated waveguide (SIW) corrugated method is introduced, which is later employed as the core component of two high gain, low mutual coupling Ka-band MIMO antennas. In [34], on top, there are two sets of four-element antenna arrays, and on the ground plane, there is a unique MTM design that improves gain, bandwidth, and mutual coupling, but the antenna structure is huge and difficult to manufacture. A slot is put between the elements of the microstrip patch antennas, reducing mutual coupling and increasing gain [35]. In [36], to enhance a circular patch MIMO antenna's bandwidth and gain, a ring and a circular parasitic antenna with an air gap were added to a conventional circular patch MIMO antenna. To improve the mutual coupling (MC) in closely packed dual-band MIMO antennas, an adapted array antenna decoupling surface and an H-shape DGS were used [37]. In [38], a proposed tri-port tiny antenna with gain enhancement was mounted on a hybrid metasurface (MS).

This work presents a rectangular slot patch MIMO antenna with good isolation and a distance from edge-to-edge of 14.5 mm. The antenna works in the 8.15 to 8.55 GHz frequency range, providing a well-known frequency standard for X-band uses. The MIMO antenna design consists of two rectangular slotted patches that emit signals, along with an FSS component. The FSS elements are positioned in a periodic arrangement around the two patches to enhance the antenna gain and minimize interference between them. Computer simulation technology (CST) is employed to design, simulate, and optimize the antenna. The antenna's performance is evaluated through both simulation and measurement, and the results are compared to assess its effectiveness.

2. ANALYSIS AND DESIGN

2.1. FSS Design

Figures 1(a) and (b) show the designed structure of the given FSS unit cell. The frequency range of the FSS is 7.0 to 9.0 GHz. The proposed FSS unit consists of a circular shape with a rectangular stub in the middle. The FSS is integrated onto the same substrate as the patch in the MIMO antenna design. The substrate, made of FR4, has a height of 1.6 mm and a dielectric constant of 4.4. The simulations are conducted using CST Microwave Studio. The FSS unit cells are designed in a closely spaced arrangement to achieve a transmission coefficient (S_{12}) below -10 dB across the entire frequency range. The dimension of the proposed unit cell in millimeters are $Rs = 3.7$, $RP = 4.2$, $LS = 4$, $WS = 0.5$, and periodicity of $p = 10$. Figures 1(c) and (d) illustrate the transmission coefficient ($|S_{21}|$) and reflection phase of the FSS unit cell, respectively. These graphs depict the functionality of the designed FSS
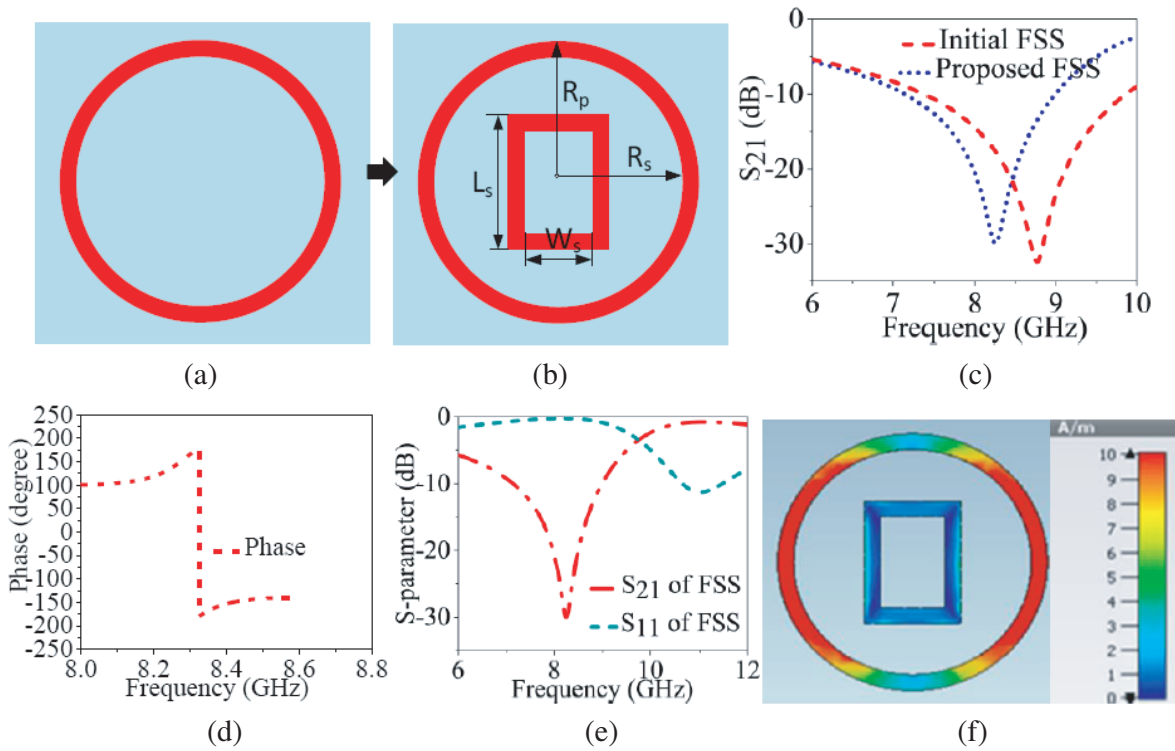
Figure 1. (a) Structure of initial and (b) proposed FSS unit cell and (c) its simulated S-parameter $|S_{21}|$ (d) phase response and (e) S-parameter $|S_{11}|$ and S-parameter $|S_{21}|$ and (f) simulated surface current distribution.

as a band-stop filter within the frequency range of 7 to 9 GHz, with a magnitude of the transmission coefficient ($|S_{21}|$) of 10 dB. The given FSS reflection phase decreases linearly with frequency and is reduced to nearly zero at 8.4 GHz. The proposed FSS exhibits a linear reflection phase throughout the frequency range of 7 to 9 GHz. Figure 1(c) depicts the two-stage development of the suggested FSS and its simulated transmission coefficient.

The evaluation of the proposed unit cell is presented in Figure 1(a) and (b). The transmission coefficient of the FSS is represented in Figure 1(c). It is obvious that in step-1, circular ring unit cell is designed, which resonates at 8.8 GHz. However, in step-2 the proposed FSS unit cell is designed by adding a rectangular stub in the circular ring, which is able to shift the resonance frequency from 8.8 GHz to the desired resonance frequency of 8.4 GHz, as depicted in Figure 1(e). In Figure 1(f), the surface current distribution of the examined antenna is depicted. The observation reveals that the metallic patch functions at the same frequency, leading to a concentrated surface current. This intensified current density causes substantial surface reflections, thereby diminishing the transmission efficiency at that specific frequency.

2.2. Antenna Design

This section designs a simple rectangular slot patch antenna for X-band application as shown in Figures 2(a)–(c). In step-1, the conventional microstrip patch antenna is made of a rectangular patch and FR-4 as a dielectric substrate with relative permittivity of 4.4 and $tan\delta = 0.025$, and the thickness is 1.6 mm with an outer dimension $W \times L = 12 \times 12\,\text{mm}^2$ as shown in Figure 2(a). During the second step of the designing antenna, a square slot is etched out from the edges, as illustrated in Figure 2(b). The simulation results, depicted in Figure 2(d), clearly demonstrate that the resonance frequency has shifted towards a higher frequency. The proposed design now exhibits resonance at 8.3 GHz.
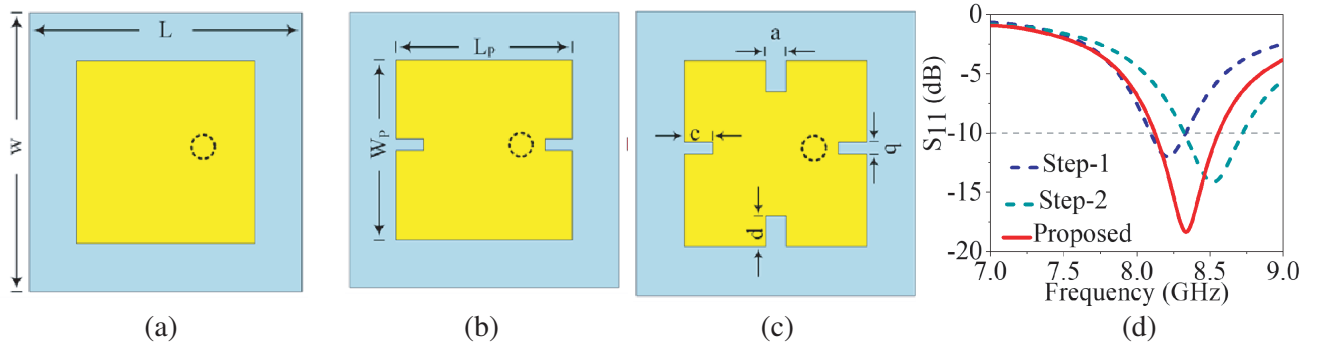
Figure 2. Design steps of proposed antenna. (a) step-1, (b) step-2, (c) proposed antenna and (d) simulated $|S_{11}|$ of different shapes of a single antenna. [$L = 12$; $W = 12$; $a = 0.36$; $b = 0.36$; $c = 1.10$; $d = 1.10$. (unit = mm).
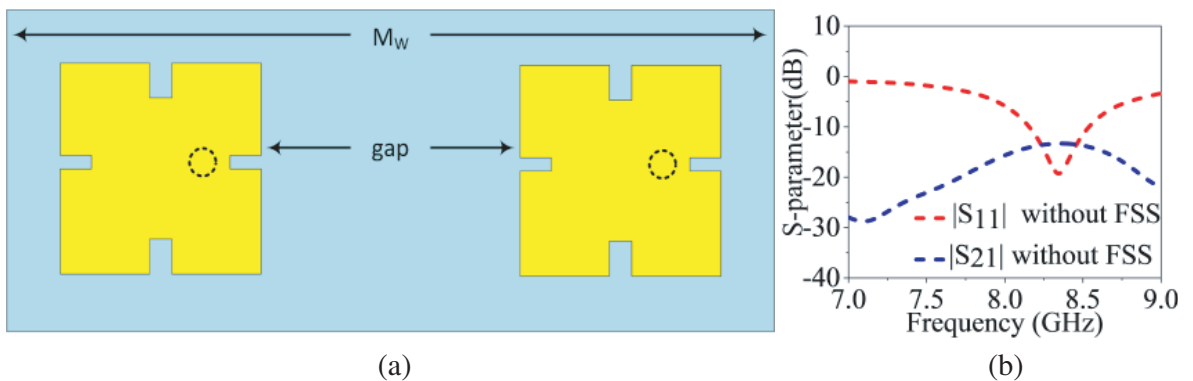
3. PROPOSED MIMO ANTENNA ANALYSIS

3.1. MIMO Antenna Design

The design and prototype models of the proposed MIMO antenna system with slotted patches are illustrated in Figure 3(a). These antenna components represent an evolution from the basic rectangular patch antenna. The specific dimensions of the proposed MIMO antenna are determined using the well established transmission line theory. This theory allows for the calculation of the effective resonant length (Ls) and width (Ws) corresponding to a given resonant frequency (f_r) [41].

$$L_{re} = \frac{c}{2f_r\sqrt{\frac{\varepsilon_r + 1}{2} + \frac{\varepsilon_r - 1}{2}\left(1 + 12\frac{h}{w}\right)^{0.5}}} - 2\Delta L \tag{1}$$

$$W = \frac{1}{2f_r\sqrt{\mu_o\varepsilon_o}}\sqrt{\frac{2}{\varepsilon_r + 1}} \tag{2}$$

The MIMO antenna's overall dimensions are $20 \times 40 \times 1.6\,\text{mm}^3$, which is smaller than other antennas. Two radiating patches with slots are fabricated on an FR-4 substrate with thickness 1.6 mm. The width and length of the radiators are 7.5 and 7.5 mm, respectively. The substrate is claimed to be supported by a shared ground plane. Initially, simple rectangular patch antenna elements were designed, each operating at 8.4 GHz with mutual coupling $|S_{21}| \leq -16\,\text{dB}$. Figure 3(b) presents the magnitudes of


Figure 3. (a) Schematic view of the proposed MIMO antenna; (b) $|S_{11}|$ and $|S_{21}|$ of MIMO antenna without FSS. [$MW = 40$; gap = 14.5. (unit = mm)].

$|S_{11}|$ and $|S_{21}|$ for the MIMO antenna without the utilization of Frequency Selective Surface (FSS). To improve the $|S_{11}|$ performance of the rectangular patch MIMO antenna, slots are introduced into the patch. By maintaining a distance of "d" between the two patches, a low mutual coupling is observed.

3.2. MIMO Antenna Using FSS

The MIMO antenna design features rectangular slotted patches and integration of FSS, as shown in Figures 4(a) and (b). The antenna components consist of two-port slotted patches that are printed on a rectangular substrate measuring $65 \times 45\,\text{mm}^2$. The antenna is fed at two ports using two $50\,\Omega$ SMA connectors. Rectangular slot patches and FSS elements are printed on the top surface of the substrate. The FSS elements are positioned periodically around the patches, with a separation distance denoted as "c", in order to improve the performance of the antenna. Impedance matching ($|S_{11}|$) is achieved across the desired resonant frequency band, which indicates good performance. Furthermore, it is also observed after loading FSS units around the antenna that the impedance matching is well preserved. Figures 4(c) and (d) show the current distributions at $8.4\,\text{GHz}$ in both the absence and presence of FSS elements. When one antenna (right side) is excited and the other antenna terminated with $50\,\Omega$ impedance, a high mutual coupling between the patches is achieved, because the current is closely linked to other radiators without FSS elements, as shown in Figure 4(c). The positioning of the FSS elements, as shown in Figure 4(d), demonstrates a noteworthy reduction in current density between the two radiating patches, yielding improved performance. Consequently, these analyses assist in identifying the optimal placement of FSS elements for enhanced isolation between the patches. By introducing FSS elements between the two patches, the flow of current to the opposite side is hindered, effectively reducing coupling between the patches. Furthermore, after loading the FSS in the middle of the two rectangular patches, the isolation, represented by $|S_{21}|$, is observed to be less than $-20\,\text{dB}$. Figures 5(a)–(c) display the $|S_{11}|$ and $|S_{21}|$ of the FSS-based antenna before and after incorporating the FSS. The


(a) (b) (c) (d)
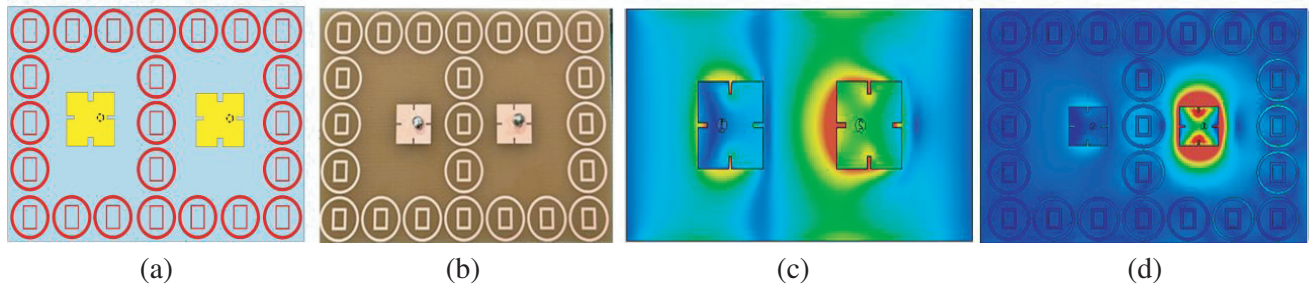
Figure 4. (a) Schematic view of MIMO antenna using FSS. (b) Fabricated prototype and (c) simulated surface current distribution without FSS and (d) with FSS.


(a) (b) (c)
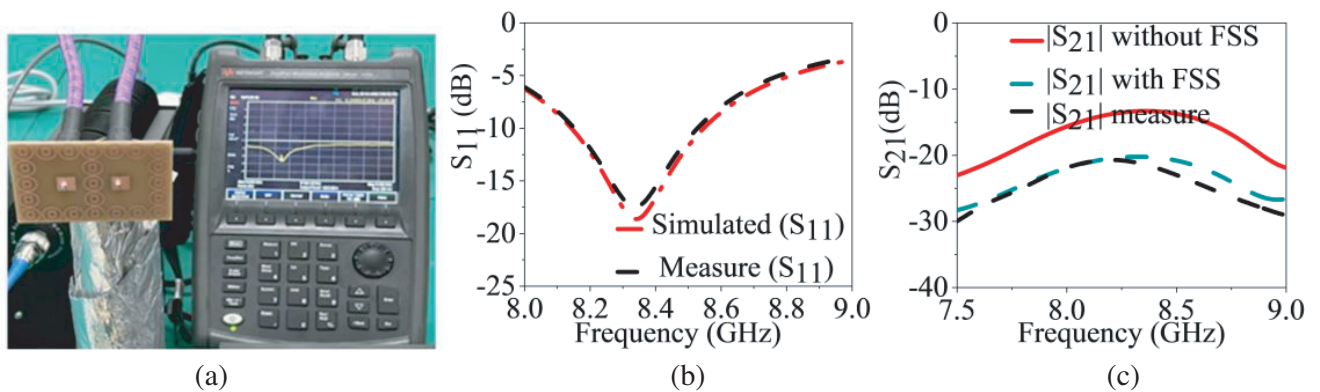
Figure 5. (a) Experimental setup. (b) Simulated and measured S_{11}. (c) S_{21}.

simulated and measured $|S_{11}|$ of the proposed MIMO antenna exhibit good agreement. Additionally, Figure 6(a) illustrates the measured and simulated gains for the two antennas. At a frequency of 8.4 GHz, the MIMO antenna exhibits a maximum gain enhancement of 2.5 dB. The antenna gain is illustrated in Figure 6(a) both with and without FSS elements. The antenna is reported to have a gain of 4 dB without FSS, but with the inclusion of FSS elements, the gain increases to 6.45 dB due to improved aperture efficiency. Placing FSS units above the MIMO antenna leads to a redistribution of surface current and facilitates the transmission of energy from the radiating element to the antenna surface. Consequently, the loaded FSS units demonstrate enhanced aperture efficiency compared to a MIMO antenna without FSS units. Notably, the FSS units surrounding the right-side patch antenna receive additional power. The integration of an FSS in the MIMO antenna leads to a significant gain improvement. This gain enhancement is achieved by the coherent superposition of energy radiated from the FSS unit cells and patches, as highlighted in the study's findings. The radiation efficiency of the antenna is depicted in Figure 6(b), demonstrating a high efficiency of approximately 77% after incorporating the FSS. To further analyze the radiation patterns of the MIMO antenna, both measured and simulated radiation patterns are presented in Figures 7(a) and (b). The results indicate that the MIMO antenna with the loaded FSS exhibits a more focused radiation pattern than the MIMO antenna without the loaded FSS.
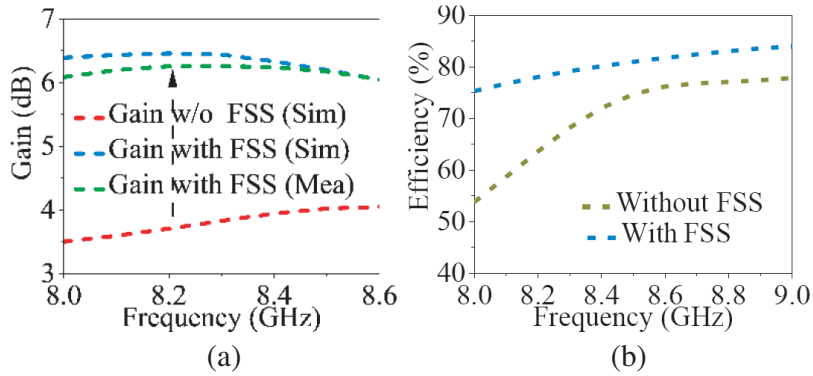
Figure 6. (a) Simulated and measured gain (b) efficiency with and without FSS.
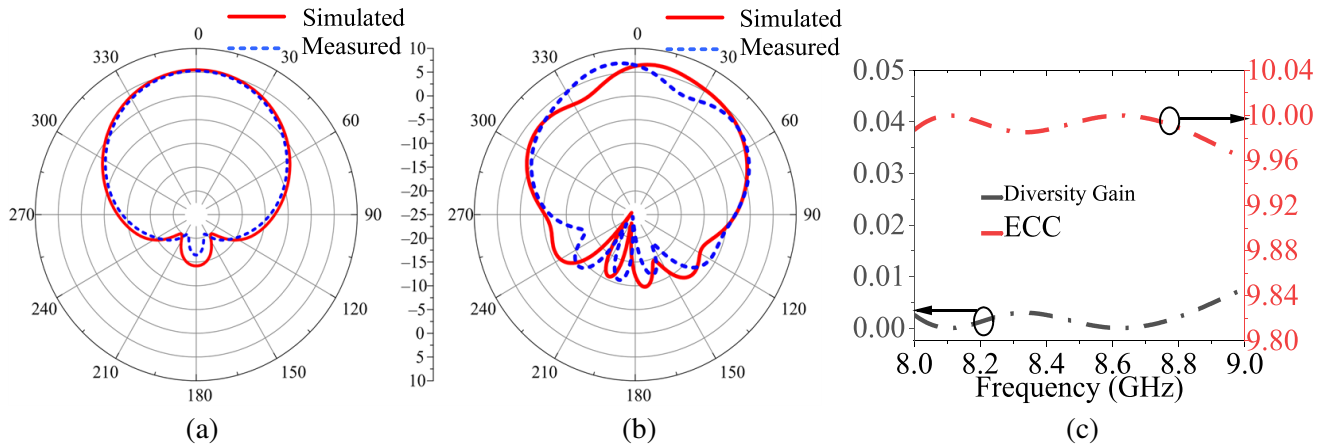
Figure 7. The radiation pattern of the proposed work, with both simulated and measured results depicted for the (a) E-plane and (b) H-plane and (c) simulated envelope correlation coefficient and diversity gain.

4. PROPOSED ANTENNA DIVERSITY PERFORMANCE

The performance evaluation of the MIMO antenna involves the consideration of established system parameters, including the Envelope Correlation Coefficient (ECC) and Diversity Gain (DG). CST Microwave Studio is utilized to estimate the diverse performance of the proposed antenna. The subsequent section provides a detailed and comprehensive explanation of these parameters.

4.1. Envelope Correlation Coefficient

Envelope Correlation Coefficient (ECC) is a critical metric for evaluating the performance of MIMO systems. In the case of the proposed antenna, ECC is utilized to assess its diversity performance, as depicted in Figure 7(c). ECC reflects the correlation between the received signals of the antenna. It can be computed using the 3D far-field radiation patterns or scattering characteristics of the antenna. It is important to note that estimating ECC values solely based on S-parameters for lossy antennas is inefficient and often leads to an underestimation of the actual requirements. Equation (3) presents the calculation of ECC for a two-port MIMO system, taking into account the S-parameters and radiation efficiency [39].

$$ECC = \frac{|S_{11} \times S_{12} + S_{21} \times S_{22}|}{(1 - |S_{11}|^2) - |S_{21}|^2 (1 - |S_{21}|^2 - |S_{22}|^2)} \tag{3}$$

The ECC, shown in Figure 7(c), indicates the correlation of the given antenna. To achieve optimal MIMO performance, it is ideal for the ECC to be below 0.5 [40]. Figure 7(c) demonstrates a minimal correlation between two antennas, with a consistently simulated ECC value below 0.001 throughout the entire operating frequency range. This observation suggests that the MIMO antenna exhibits remarkable pattern diversity, as the ECC value is below 0.5.

4.2. Diversity Gain

The Diversity Gain (DG) in wireless networks serves as a measure of performance and reliability for MIMO antennas. It is typically achieved by receiving multiple transmission streams through distinct channel paths. Therefore, the MIMO antenna should demonstrate a high DG, ideally exceeding 10 dB,

Table 1. Comparison of the given work with previously published works.

References	f (GHz)	Ant. Dimension (mm^2)	BW (%)	Gain (dB)	Layer	Method
[15]	10.44	28 × 28	6.93	7.57	2	Metasurface superstrate
[16]	2.4	120 × 120	-	10.14	2	FSS superstrate
[17]	4–12	86.5 × 86.5	-	12	2	FSS
[18]	2.5–12	82.5 × 82.5	-	9	2	FSS Reflector
[19]	2.45–5.8	76 × 52	5.48 to 7.48	5	2	FSS
[20]	5.79–6.02	29.2 × 41	6.93	5.37	2	Metameterial array
[30]	26	30 × 30.5	-	7.4	2	metamaterial
[31]	26.8–28.4	72 × 17.2	5.8	69.5	1	Parasitic element
[32]	5.8	137 × 77	-	9.2	2	Metameterial
[34]	2.3	50 × 130	49.7	7.1	1	Parasitic structure
[35]	3.7–4.1	48.5 × 60.6		8.1	2	MADS and HDGS
[37]	1.3–40	47.5 × 40.1	187	8.51	1	T-shape Parasitic
[38]	4–8	80 × 40	65.5	3.8	1	Metasurface DMS
Prop.	8.4	65 × 45	6.45	6.5	1	Single substrate

within the designated frequency range, as shown in Figure 7(c). The DG can be calculated using Equation (4), with the ECC value as one of the parameters [42].

$$DG = 10 \times \sqrt{1 - (ECC)^2} \tag{4}$$

Table 1 provides a comparison of the proposed MIMO antenna's performance with recently published works in the literature, focusing on the antenna's size, isolation, and high gain. The proposed MIMO antenna exhibits high gain, compact size, and maintains satisfactory isolation between its radiators. The comparison includes various aspects such as overall antenna volume, isolation, mutual coupling reduction, and gain enhancement techniques. It can be observed from Table 1 that the antenna [16] achieves high gain but has a narrow bandwidth, a two-layer construction, and a significantly larger size than the proposed antennas [17, 18], which also have larger sizes. On the other hand, the antenna in [15] demonstrates a smaller size but features a two-layer construction and lower gain than the given antenna. The proposed design stands out as it utilizes a single substrate, unlike other antenna designs that involve multiple substrates, as indicated in Table 1. While alternative methods may enhance antenna gain, they often come with increased complexity, larger footprint, and potential impacts on other parameters such as radiation pattern and efficiency. Consequently, the antenna's overall cost may rise due to its complexity. In this study, the antenna and reflector are designed on the same substrate, minimizing space requirements and improving radiation performance.

5. CONCLUSION

This study presents a single-band slotted patch MIMO antenna aimed at enhancing isolation and gain. The MIMO antenna features a simple design with compact dimensions of $65 \times 45 \, \text{mm}^2$ and a gap of $14.5 \, \text{mm}$ between the two patches. To improve the gain and reduce mutual coupling, a novel approach utilizing an angularly stable band-stop FSS is employed. Metasurfaces, known for their exceptional electromagnetic properties, are utilized to enhance performance and reduce the size of patch antennas. The proposed FSS consists of a periodic structure with a circular shape and a rectangular stub in the center. It exhibits high stability across various polarizations and incidence angles. The operating frequency range of the FSS spans from 7 to 9 GHz. The FSS elements are strategically positioned periodically around the two antennas to improve impedance matching, reduce mutual coupling, and enhance gain. The antenna demonstrates an impedance bandwidth ranging from 8.0 to 8.55 GHz, with significant isolation of 21 dB within the resonating band. At 8.4 GHz, the antenna achieves a peak gain of 6.5 dB and radiation efficiency of 77%. The ECC indicates exceptional diversity performance, with a value of 0.001, while the DG achieves an impressive approximately 10 dB. Instead of utilizing multiple substrates for the antenna and FSS, which occupies considerable space, the suggested approach integrates both the antenna and FSS on a single substrate. This innovation leads to enhanced performance and compactness, offering a more efficient solution.

REFERENCES

1. Hussain, M., W. A. Awan, E. M. Ali, M. S. Alzaidi, M. Alsharef, D. H. Elkamchouchi, A. Alzahrani, and M. Fathy Abo Sree, "Isolation improvement of parasitic element-loaded dual-band MIMO antenna for mm-wave applications," *Micromachines*, Vol. 13, 1918, 2022.

2. Bayarzaya, B., N. Hussain, W. A. Awan, M. A. Sufian, A. Abbas, D. Choi, J. Lee, and N. Kim, "A compact MIMO antenna with improved isolation for ISM, sub-6 GHz, and WLAN application," *Micromachines*, 2022, Vol. 13, 1355.

3. Rahman, S. U., Q. Cao, F. Amin, et al., "Multifunctional polarization converting metasurface and its application to reduce the radar cross-section of an isolated MIMO antenna," *Journal of Physics D: Applied Physics*, Vol. 53, No. 30, 305001, 2020.

4. Khan, M. I., M. I. Khattak, S. U. Rahman, A. B. Qazi, A. A. Telba, and A. Sebak, "Design and investigation of modern UWB-MIMO antenna with optimized isolation," *Micromachines*, Vol. 11, No. 4, 432, 2020.

5. Ahmad, A., A. Ullah, C. Feng, M. Khan, S. Ashraf, M. Adnan, S. Nazir, and H. U. Khan, "Towards an improved energy efficient and end-to-end secure protocol for iot healthcare applications," *Security and Communication Networks*, Vol. 2020, 1–10, 2020.

6. Hussain, N., W. A. Awan, W. Ali, S. I. Naqvi, A. Zaidi, and T. T. Le, "Compact wideband patch antenna and its MIMO configuration for 28 GHz applications," *AEU Int. J. Electron. Commun.*, Vol. 132, 153612, 2021.

7. Ibrahim, A. A., M. A. Abdalla, A. B. Abdel-Rahman, and H. F. Hamed, "Compact MIMO antenna with optimized mutual coupling reduction using DGS," *Int. J. Microw. Wirel. Technol.*, Vol. 6, 173–180, 2014.

8. Sabaawi, A. M. A., K. S. Muttair, O. A. Al-Ani, and Q. H. Sultan, "Dual-band MIMO antenna with defected ground structure for sub-6 GHz 5G applications," *Progress In Electromagnetics Research C*, Vol. 122, 57–66, 2022.

9. Gong, Y.-Y., L. Wang, and Z. Zhang, "The novel Y shaped fractal defected ground structure for the mutual coupling reduction," *Progress In Electromagnetics Research M*, Vol. 72, 13–21, 2018.

10. Yang, Y., Q. Chu, and C. Mao, "Multiband MIMO antenna for GSM, DCS, and LTE indoor applications," *IEEE Antennas Wirel. Propag. Lett.*, Vol. 15, 1573–1576, 2016.

11. Sun, Y., M. Tian, and G. S. Cheng, "Characteristic mode-based neutralization line design for MIMO antenna," *International Journal of Antennas and Propagation*, Jul. 30, 2022.

12. Ou Yang, J., F. Yang, and Z. Wang, "Reducing mutual coupling of closely spaced microstrip MIMO antennas for WLAN application," *IEEE Antennas Wirel. Propag. Lett.*, Vol. 10, 310–313, 2011.

13. Hussain, M., Q. Abbas, S. H. H. Gardzi, M. Alibakhshikenari, F. Falcone, and E. Limiti, "Ultra-wideband MIMO antenna realization for indoor Ka-band applications," *2022 United States National Committee of URSI National Radio Science Meeting (USNC-URSI NRSM)*, 108–109, 2022.

14. Saravanan, M., V. B. Geo, and S. M. Umarani, "Gain enhancement of patch antenna integrated with metamaterial inspired superstrate," *J. Electr. Sys. Info. Technol.*, Vol. 5, 263–270, 2018.

15. Samantaray, D. and S. Bhattacharyya, "A gain-enhanced slotted patch antenna using metasurface as superstrate configuration," *IEEE Trans. Antennas Propag.*, Vol. 68, 6548–6556, 2020.

16. Arnmanee, P. and C. Phongcharoenpanich, "Improved microstrip antenna with HIS elements and FSS superstrate for 2.4 GHz band applications," *Int. J. Antennas Propag.*, Vol. 2018, 1–11, 2018.

17. Kushwaha, N., R. Kumar, and T. Oli, "Design of a high-gain ultra-wideband slot antenna using frequency selective surface," *Microwave Opt. Technol. Lett.*, Vol. 56, 1498–1502, 2014.

18. Yuan, Y., X. Xi, and Y. Zhao, "Compact UWB FSS reflector for antenna gain enhancement," *IET Microwaves Antennas Propag.*, Vol. 13, 1749–1755, 2019.

19. Hsing-Yi, C., Tao Y. "Bandwidth enhancement of a U-slot patch antenna using dual-band frequency-selective surface with double rectangular ring elements," *Microwave Opt. Technol. Lett.*, Vol. 53, 1547–1553, 2011.

20. Adelson, M. L., O. N. Henrique, H. O. C. Nilson, and J. P. da-Silva, "Effect of metamaterial cells array on a microstrip patch antenna design," *J. Microwaves Optoelectron. Electromag. Appl.*, Vol. 19, 327–342, 2020.

21. Adibi, S., M. A. Honarvar, and A. Lalbakhsh, "Gain enhancement of wideband circularly polarized UWB antenna using FSS," *Radio Sci.*, Vol. 56, e2020RS007098, 2021.

22. Afzal, M. U., A. Lalbakhsh, and K. P. Esselle, "Electromagnetic-wave beam-scanning antenna

using near-field rotatable graded-dielectric plates," *J. App. Phy.*, Vol. 124, 234901–234911, 2018.

23. Mackay, A., B. Sanz-Izquierdo, and E. A. Parker, "Evolution of frequency selective surfaces," *Forum for Electromagnetic Research Methods and Application Technologies (FERMAT)*, Vol. 2, 1–7, 2014.

24. Nair, R. U. and R. M. Jha, "Electromagnetic design and performance analysis of airborne radomes: Trends and perspectives antenna applications corner," *Anten. Propag. Mag.*, Vol. 56, 276–298, 2014.

25. Luukkonen, O., F. Costa, C. R. Simovski, A. Monorchio, and S. A. Tretyakov, "A thin electromagnetic absorber for wide incidence angles and both polarizations," *IEEE Trans. Antennas Propag.*, Vol. 57, 3119–3125, 2009.

26. Zahirjoozdani, M., M. Khalajamirhosseini, and A. Abdolali, "Wideband radar cross-section reduction of patch array antenna with miniaturized hexagonal loop frequency selective surface," *Electron. Lett.*, Vol. 52, 767–768, 2016.

27. Hiranandani, M. A., A. B. Yakovlev, and A. A. Kishk, "Artificial magnetic conductors realized by frequency-selective surfaces on a grounded dielectric slab for antenna applications," *IEEE Proc. Microw. Antennas Propag.*, Vol. 153, 487–493, 2006.

28. Mark, R., N. Rajak, K. Mandal, and S. Das, "Isolation and gain enhancement using metamaterial-based super-strate for MIMO applications," *Radioengineering*, Vol. 28, No. 4, 689–695, 2019.

29. Peng, H., R. Zhi, Q. Yang, J. Cai, Y. Wan, and G. Liu, "Design of a MIMO antenna with high gain and enhanced isolation for WLAN applications," *Electron.*, Vol. 10, No. 14, 1659, 2021.

30. Jiang, H., L. M. Si, W. Hu, and X. Lv, "A symmetrical dual-beam bowtie antenna with gain enhancement using metamaterial for 5G MIMO applications," *IEEE Photonics J.*, Vol. 11, No. 1, 1–9, 2019.

31. Lin, M., P. Liu, and Z. Guo, "Gain-enhanced Ka-band MIMO antennas based on the SIW corrugated technique," *IEEE Antennas Wirel. Propag. Lett.*, Vol. 16, 3084–3087, 2017.

32. Nguyen, N. L., "Gain enhancement for MIMO antenna using metamaterial structure," *Int. J. Microw. Wirel. Technolo.*, Vol. 11, No. 8, 851–862, 2019.

33. Khajeh-Khalili, F., M. A. Honarvar, M. Naser-Moghadasi, and M. Dolatshahi, "Gain enhancement and mutual coupling reduction of multiple-intput multiple-output antenna for millimeter-wave applications using two types of novel metamaterial structures," *Int. J. RF Microw. Comp. Aided Eng.*, Vol. 30, No. 1, e22006, 2020.

34. Firmansyah, T., H. Herudin, S. Suhendar, R. Wiryadinata, M. I. Santoso, Y. R. Denny, and T. Supriyanto, "Bandwidth and gain enhancement of MIMO antenna by using ring and circular parasitic with air-gap microstrip structure," *TELKOMNIKA*, Vol. 15, No. 3, 1155–1163, 2017.

35. Niu, Z., H. Zhang, Q. Chen, and T. Zhong, "Isolation enhancement in closely coupled dual-band MIMO patches antennas," *IEEE Antennas Wirel. Propag. Lett.*, Vol. 18, No. 8, 1686–1690, 2019.

36. Mohanty, A., B. R. Behera, and N. Nasimuddin, "Hybrid metasurface loaded tri-port compact antenna with gain enhancement and pattern diversity," *Int. J. RF Microw. Comp. Aided Eng.*, Vol. 31, No. 11, e22795, 2021.

37. Ullah, H., S. U. Rahman, Q. Cao, I. Khan, and H. Ullah, "Design of SWB MIMO antenna with extremely wide-band isolation," *Electron.*, Vol. 9, No. 1, 194, 2020.

38. Jabire, A. H., H. X. Zheng, A. Abdu, and Z. Song, "Characteristic mode analysis and design of wide band MIMO antenna consisting of metamaterial unit cell," *Electron.*, Vol. 8, No. 1, 68, 2019.

39. Khan, I., K. Zhang, Q. Wu, I. Ullah, L. Ali, H. Ullah, and S. U. Rahman, "A wideband high-isolation microstrip MIMO circularly-polarized antenna based on parasitic elements," *Materials*, Vol. 16, No. 1, 103, Jan. 2023.

40. Rahman, S. U., H. Deng, M. Sajjad, A. Rauf, Z. Shafiq, M. Ahmad, and S. Iqbal, "Angularly stable frequency selective surface for the gain enhancement of isolated multiple input multiple output antenna," *Microwave Opt. Technol. Lett.*, Vol. 63, No. 11, 2803—2810, Nov. 2021.

41. Balanis, C. A., *Antenna Theory: Analysis and Design*, John Wiley & Sons, 2016.

42. Khan, I., Q. Wu, I. Ullah, S. U. Rahman, H. Ullah, and K. Zhang, "Designed circularly polarized two-port microstrip MIMO antenna for WLAN applications," *Applied Sciences*, Vol. 12, No. 3, 1068, Jan. 20, 2022.